C 23rd Conference on Application of Accelerators in Research and Industry, CAARI 2014

Thermoelectric Figures of Merit of Zn₄Sb₃ and Zrnisn-Based Half-Heusler Compounds Influenced by Mev Ion-Beam Bombardments

S. Budak[a*], S.Guner[b], C. I. Muntele[c], D. Ila[d]

[a] Department of Electrical Engineering and Computer Science, Alabama A&M University, Normal, AL 35762, USA
[b] Department of Physics, Fatih University, 34500, B. Cekmece / Istanbul, Turkey
[c] Cygnus Scientific Services, Huntsville, AL 35815, USA
[d] Department of Physics, Fayetteville St. University, Fayetteville, NC USA

Abstract

Semiconducting β-Zn_4Sb_3 and ZrNiSn-based half-Heusler compound thin films with applications as thermoelectric (TE) materials were prepared using ion beam assisted deposition (IBAD). High-purity solid zinc (Zn) and antimony (Sb) were evaporated by electron beam to grow the β-Zn_4Sb_3 thin film while high-purity zirconium (Zr) powder and nickel (Ni) tin (Sn) powders were evaporated by electron beam to grow the ZrNiSn-based half-Heusler compound thin film. Rutherford backscattering spectrometry (RBS) was used to analyze the composition of the thin films. The grown thin films were subjected to 5 MeV Si ions bombardment for generation of nanostructures in the films. We measured the thermal conductivity, Seebeck coefficient, and electrical conductivity of these two systems before and after 5 MeV Si ions beam bombardment. The two material systems have been identified as promising TE materials for the application of thermal-to-electrical energy conversion, but the efficiency still limits their applications. The electronic energy deposited due to ionization in the track of MeV ion beam could cause localized crystallization. The nanostructures produced by MeV ion beam can cause significant change in both the electrical and the thermal conductivity of thin films, thereby improving the efficiency. We used the 3ω-method (3rd harmonic) measurement system to measure the cross-plane thermal conductivity, the van der Pauw measurement system to measure the electrical conductivity, and the Seebeck-coefficient measurement system to measure the cross-plane Seebeck coefficient. The thermoelectric figures of merit of the two material systems were then derived by calculations using the measurement results. The MeV ion-beam bombardment was found to decrease the thermal conductivity of thin films and increase the efficiency of thermal-to-electrical energy conversion.

Keywords: Ion bombardment; thermoelectric properties; thin films; RBS; Figure of merit.

*Corresponding author: Tel.: 256-372-5894; Fax: 256-372-5855
Email: satilmis.budak@aamu.edu

1. Introduction

Thermoelectric materials are getting importance due to their applications in thermoelectric power generation and microelectronic cooling [1]. An important application of thermoelectric materials is in direct thermal-to-electrical energy conversion. Because a substantial amount of energy in our world is in thermal form, there are tremendous applications for thermoelectric devices that efficiently convert thermal energy into electricity [2]. There are three thermoelectric materials which are based on ANiSn (A=Ti, Zr, Hf) compounds and their alloys. These three compounds are members of a larger family of ternary intermetallic compounds ABX, where A is a transition metal of left-hand side of periodic table (titanium or vanadium group elements), B is a transition metal of the right-hand side of the periodic table (iron, cobalt, or nickel group elements), and X is one of the main group elements, Ga, Sn, or Sb [3]. Thermoelectric power generation could convert heat to electricity directly. The ZrNiSn half-Heusler alloy is one of the potential candidates for the thermoelectric materials and has recently received great interest [4]. β-Zn_4Sb_3 with a complex hexagonal crystal structure has also been discovered to be one of the promising candidates for thermoelectric power generation applications [5]. Two phases in the Zn-Sb system, β-Zn_4Sb_3 and ZnSb, are well known as good thermoelectric materials. The constituent elements of ZnSb are low cost and non-toxic, and an abundant. ZnSb is therefore more environmentally sound than lead telluride, which is toxic [6, 7]. The figure of merit (ZT) of β-Zn_4Sb_3 is the highest in a temperature range from 200 ^{O}C to 400 ^{O}C among the known thermoelectric materials. In the Zn-Sb binary system, ZnSb is already known as a thermoelectric material and its properties were investigated 40 - 50 years ago. ZnSb has a large figure of merit, while Zn is a typical metal with a good electrical conductivity but a low Seebeck coefficient [8]. Effectiveness of the thermoelectric materials depends on a low thermal conductivity and a high electrical conductivity [9, 10]. The performance of the thermoelectric materials and devices is described by a dimensionless figure of merit, $ZT = S^2 \sigma T / \kappa$ where S is the Seebeck coefficient, σ is the electrical conductivity, T is the absolute temperature, and κ is the thermal conductivity [11-13]. Higher *ZT* can be reached by increasing S, increasing σ, or decreasing κ. Since the bulk form of the half-Heusler β-Zn_4Sb_3 has a higher figure of merits at higher temperatures [14] and the half-Heusler ZrNiSn has been studied by many researchers for the candidate as the practical thermoelectric materials because of their good thermoelectric performance and low toxicity of the constituent elements [15], we worked on the thin films of these materials. We have performed some initial studies related to Zn_4Sb_3 thin films and Zn_4Sb_3 multilayer composition with $CeFe_{(4-x)}Co_xSb_{12}$ in ref.[16, 17]. We have reached the figure of merit of 0.0017 for Zn_4Sb_3 / $CeFe_2Co_2Sb_{12}$ multilayer system [16] and the figure of merit of 0.20 for the 383 nm Zn_4Sb_3 thin films [17]. Improving in the figure of merit in the previous studies directed us to continue on these samples at different thicknesses. In this study, we reported on the growth of half-Heusler alloys of Zn_4Sb_3 and ZrNiSn thin films on the silica substrates using an ion-beam assisted deposition (IBAD), and high energy Si ions bombardments of the thin films for reducing thermal conductivity and increasing electrical conductivity.

2. Experimental

Semiconducting β-Zn_4Sb_3 and ZrNiSn-based half-Heusler compound thin films on the silicon and silica (suprasil) substrates were grown with the ion beam assisted deposition (IBAD). High-purity solid zinc and antimony were evaporated by electron beam to grow the β-Zn_4Sb_3 thin film while high-purity zirconium powder and nickel tin powders were evaporated by electron beam to grow the ZrNiSn-based half-Heusler compound thin film. The thicknesses of the films were controlled by an INFICON deposition monitor. The film geometries used in this study are shown in Fig.1. Fig.1a shows the geometry of Zn_4Sb_3 thin film from the cross-section while Fig.1b shows the geometry of ZrNiSn thin film. The geometries in Fig.1 show two Au contacts on the top and the bottom of the films. These two Au contacts were used in the Seebeck coefficient measurements.
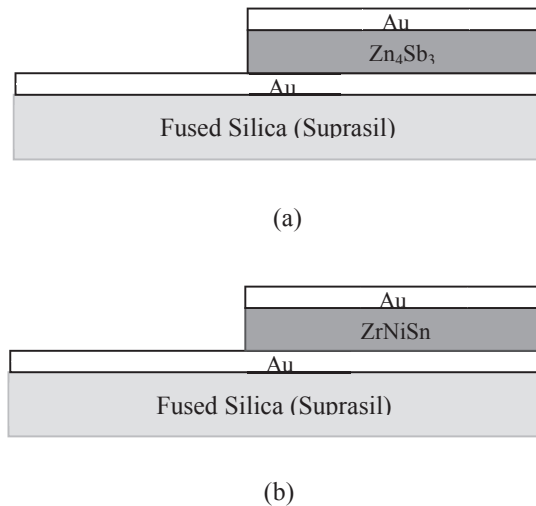
(a)

(b)

Fig. 1. Geometry of sample from the cross-section.

The electrical conductivity was measured by the van der Pauw system and the thermal conductivity was measured by the 3ω technique (3rd harmonic). The electrical conductivity, the thermal conductivity and the Seebeck measurements were performed at a room temperature of 22 ° C. One could find detailed information about 3ω technique in Refs. [18-20]. The 5 MeV Si ions bombardment was used by the Pelletron ion beam accelerator at the Alabama A&M University's Materials Research Laboratory (AAMU-MRL). The fluences used for the bombardments were ($1*10^{14}$ ions/cm^2), ($5*10^{14}$ ions/cm^2), ($1*10^{15}$ ions/cm^2), ($5*10^{15}$ ions/cm^2) and ($8*10^{15}$ ions/cm^2). Rutherford backscattering spectrometry (RBS) measurement was performed using 2.1 MeV He$^+$ ions in an IBM scattering geometry with the particle detector placed at 170 ^{O} from the incident beam to monitor the film thickness and stoichiometry before and after 5 MeV Si ions bombardments [21, 22].

3. Results and Discussion

Fig. 2a shows RBS spectrum of Zn$_4$Sb$_3$ thin film on Glassy Polymeric Carbon (GPC) substrate when the sample is at the normal angle. RUMP simulation [23] gives information about the amount of the elements in the deposited samples and the thickness of the deposited films. According to the RUMP simulation for Zn$_4$Sb$_3$ thin film, the ratio between Zn and Sb was found as 4:3, and the thickness of the Zn$_4$Sb$_3$ was found as 680 nm. Fig. 2b shows RBS spectrum of ZrNiSn thin film on Glassy Polymeric Carbon (GPC) substrate when the sample is at the normal angle. The RUMP simulation for ZrNiSn gave the thickness of 110 nm. The initial studies related to these films have been already published elsewhere [24].

Fig. 3 shows the penetration depth of Si ions in the Zn$_4$Sb$_3$ (fig.3a) and ZrNiSn (fig.3b) thin films. As seen from figure 3a, high energy Si ions bombardment passes through in the thin film of Zn$_4$Sb$_3$ with the damaging and ends through the substrate. The figure gives us an idea how much effects were distributed through the thin film structure. Figure 3b shows the Si ions effect on ZrNiSn thin film structure. Since the thicknesses of these two thin film structures are much different than from each other, the more effect could be seen in the thicker film through the high energy ion path while it is traveling through the thickness of the thin film. Figure 4 shows the thermoelectric properties of these two thin film structures. The figure of merit for the thicker film of Zn$_4$Sb$_3$ looks bigger than the thin film of ZrNiSn. More damage in the multilayer thin film structure could bring more positive effects in the change of the thermoelectric properties.
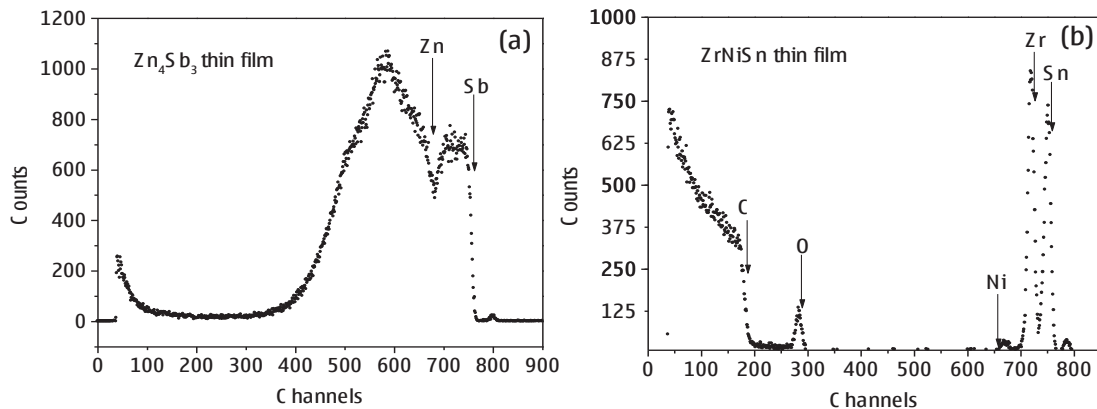
Fig. 2. He$^+$ RBS spectra of Zn$_4$Sb$_3$ and ZrNiSn films on GPC substrate.
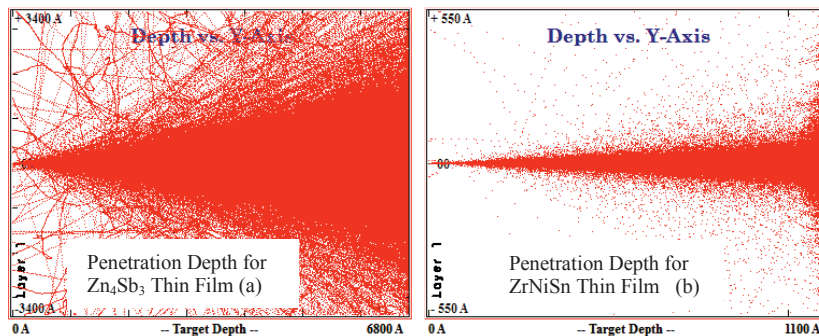

Fig. 3. The penetration depth of Si ions in the Zn$_4$Sb$_3$ (fig.3a) and ZrNiSn (fig.3b) thin films.

Fig. 4 shows the thermoelectric properties of Zn$_4$Sb$_3$ and ZrNiSn thin films. Fig. 4a shows the square of the Seebeck coefficient change for Zn$_4$Sb$_3$ thin film depending on the fluences of the bombardments. As seen from Fig.4a, the square of the Seebeck coefficient for Zn$_4$Sb$_3$ thin film tends to decrease starting from the virgin case of the Zn$_4$Sb$_3$ thin film to the fluence of ($5*1014$ ions/cm2). After the fluence of $5*1014$ ions/cm^2, the square of the Seebeck coefficients started to increase. The requirement of a high Seebeck coefficient is natural since S is a measure of the average thermal energy which is carried per charge (electron or hole) [25].

Fig. 4b shows the electrical conductivity change for Zn$_4$Sb$_3$ thin film depending on the fluences. As seen from fig. 4b, the electrical conductivity for Zn$_4$Sb$_3$ thin film started to increase when the first bombardment of $1*10^{14}$ ions/cm^2 was introduced. After the fluence of $1*10^{14}$ ions/cm^2, the electrical conductivity for Zn$_4$Sb$_3$ thin film started to decrease until the fluence of $5*10^{14}$ ions/cm^2. After the fluence of $5*10^{14}$ ions/cm^2, the electrical conductivity for Zn$_4$Sb$_3$ thin film started to increase. The electrical conductivity increased until the fluence of $1*10^{15}$ ions/cm^2. After the fluence of $1*10^{15}$ ions/cm^2, the electrical conductivity decreased depending on the applied fluence of the bombardment. The fluences of $1*10^{14}$ ions/cm^2, $5*10^{14}$ ions/cm^2 , and $1*10^{15}$ ions/cm^2 behaved as turning points for the electrical conductivity for Zn$_4$Sb$_3$ thin film. This shows that ion bombardment caused an increase in the electrical conductivity until one certain fluence was reached. While the virgin sample (unbombarded) is being bombarded with the 5 MeV Si ions, the numbers of the charge carriers in both the conduction and valence bands increase. This increase causes shorter energy gap between the conduction and valence bands. The shorter energy gap causes increase in the electrical conductivity. The decrease in the electrical conductivity might be due to the degenerations in both the conduction and the valence bands. The increase in the electrical conductivity is one of

the desired conditions for both the thermoelectric materials and the devices. Fig. 4c shows the thermal conductivity change for Zn_4Sb_3 thin film depending on the fluences. As seen from fig. 4c, the thermal conductivity for Zn_4Sb_3 thin film decreases starting from the virgin case to the fluence of $5*10^{14}$ ions/cm^2. The decrease in the thermal conductivity is another desired property in both the thermoelectric materials and devices. After the fluence of $5*10^{14}$ ions/cm^2, the thermal conductivity for Zn_4Sb_3 thin film increases until the fluence of $5*10^{15}$ ions/cm^2. After the fluence of $5*10^{15}$ ions/cm^2, the thermal conductivity started to decrease again. The high energy ion bombardment can produce nanostructures and modify the property of thin films [26], resulting in lower thermal conductivity and higher electrical conductivity. Zn_4Sb_3 has recently been investigated the most owing to its remarkably low thermal conductivity. However, ZnSb may be more stable, and with the promise of nano-structuring, it can be reconsidered for applications provided that the thermal conductivity can be reduced while maintaining a high electrical conductivity [27]. Fig. 4d shows the fluence dependence of figure of merit of Zn_4Sb_3 thin film. As seen from fig. 4d, the figure of merit value started to increase when the 5 MeV Si ions bombardment was introduced until the fluence of $1*10^{14}$ ions/cm^2. After the fluence of $1*10^{14}$ ions/cm^2, the figure of merit started to decrease. Both the good thermoelectric materials and devices should have higher figure of merit. The figure of merit for Zn_4Sb_3 thin film increases from 0.176 at zero fluence to 0.53 at $1*10^{14}$ ions/cm^2 fluence. After the fluence of $1*10^{14}$ ions/cm^2, the figure of merit decreases to 0.032 at $1*10^{15}$ ions/cm^2 fluence and after this fluence the figure of merit continues to decrease until the fluence of $5*10^{15}$ ions/cm^2. After the fluence of $5*10^{15}$ ions/cm^2, the figure of merit started to increase. L. T. Zhang et al., studied the temperature dependence of thermoelectric properties of ZnSb and Zn inclusions of studies of β-Zn_4Sb_3 samples. They have reached an increase in both the Seebeck coefficient and electrical conductivity and decrease in the thermal conductivity in the temperature variation [8]. Many other researchers studied also the temperature and doping effects of ZnSb and β-Zn_4Sb_3 samples. They got positive effects of temperature annealing and some metal doping on the thermoelectric properties of ZnSb and β-Zn_4Sb_3 samples [6, 7, and 27].
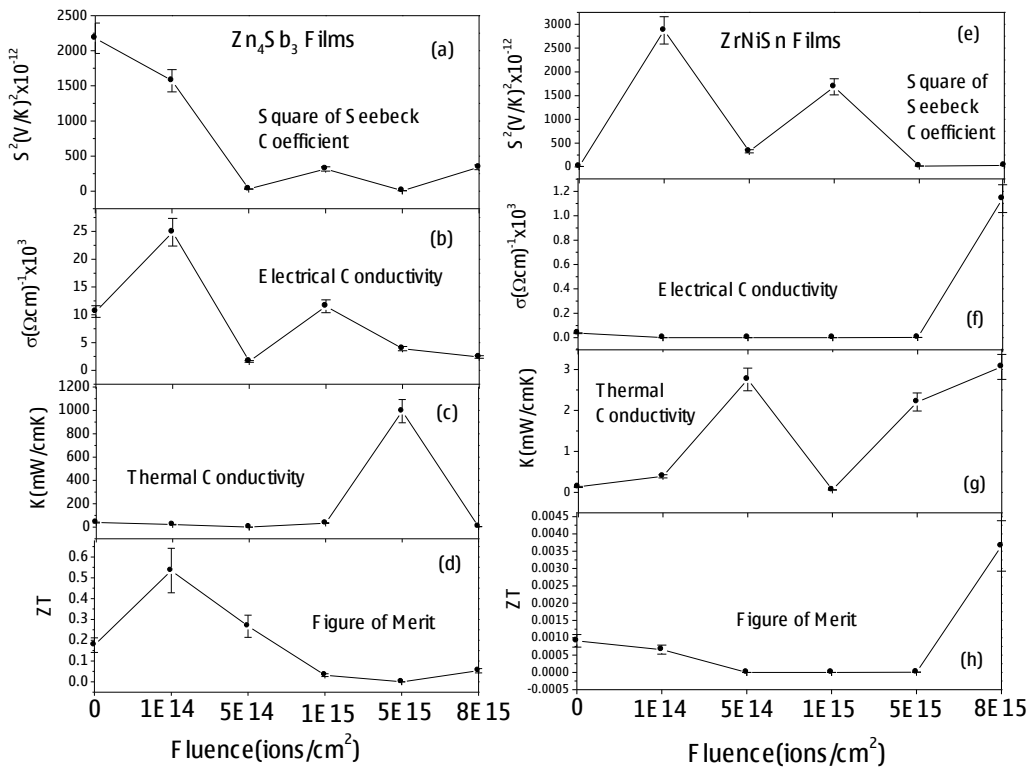

Fig.4. Thermoelectric properties of Zn_4Sb_3 and ZrNiSn thin films.

Fig. 4e shows the square of the Seebeck coefficient change for ZrNiSn thin film depending on the fluences of the bombardments. As seen from fig.4e, the square of the Seebeck coefficient for ZrNiSn thin film tends to increase starting from the virgin case of the ZrNiSn thin film to the fluence of $1*10^{14}$ ions/cm^2. After the fluence of $1*10^{14}$ ions/cm^2, the square of the Seebeck coefficient started to decrease until the fluence of $5*10^{14}$ ions/cm^2. After the fluence of $5*10^{14}$ ions/cm^2, the square of the Seebeck coefficient for ZrNiSn thin film increases until the fluence of $1*10^{15}$ ions/cm^2. After the fluence of $1*10^{15}$ ions/cm^2, the square of the Seebeck coefficient started to decrease. Fig. 4f shows the electrical conductivity change for ZrNiSn thin film depending on the fluences. As seen from fig. 4f, the electrical conductivity for ZrNiSn thin film decreased when the first bombardment of $1*10^{14}$ ions/cm^2 was introduced. After the fluence of $1*10^{14}$ ions/cm^2, the electrical conductivity for ZrNiSn thin film kept constant at around zero. The decrease in the electrical conductivity might be due to the degenerations in both the conduction and the valence bands. After the fluence of the $5*10^{15}$ ions/cm^2, the electrical conductivity started to increase. Fig. 4g shows the thermal conductivity change for ZrNiSn thin film depending on the fluences. As seen from fig. 4g, the thermal conductivity for ZrNiSn thin film increases starting from the virgin case to the fluence of $5*10^{14}$ ions/cm^2. After the fluence of $5*10^{14}$ ions/cm^2, the thermal conductivity for ZrNiSn thin film decreases until the fluence of $1*10^{15}$ ions/cm^2. After the fluence of $1*10^{15}$ ions/cm^2, the thermal conductivity started to increase. Fig. 4h shows the fluence dependence of figure of merit of ZrNiSn thin film. As seen from fig. 4h, the figure of merit value started to decrease when the 5 MeV Si ions bombardment was introduced until the fluence of $5*10^{14}$ ions/cm^2. After the fluence of $5*10^{14}$ ions/cm^2, the figure of merit kept constant at around $5.93x10^{-7}$. The figure of merit for ZrNiSn thin film decreases from $9.11x10^{-4}$ at zero fluence   to $5.93x10^{-7}$ at $1*10^{15}$ ions/cm^2 fluence. After the fluence of $8*10^{15}$ ions/cm^2, the figure of merit started to increase up to the value of 0.0038. Hiroaki et al., studied the substitution effect on the thermoelectric properties of ZrNiSn compounds. They have reached positive effects of substitution of Ti, Hf, Pd and Pt on the thermoelectric properties. Their electrical and thermal conductivity values decreased depending on the substitution and temperature change [28]. Pengfei Qiu et al., studied effect of antisite defects on the band structure and thermoelectric performance of ZrNiSn half-Heusler alloys. The temperature change affects the thermoelectric properties in the positive direction. When they added Hf, Pd and Sn, the figure of merit values decreased [29]. Xiao-Hua Liu et al., synthesized $Zr_{1-x}Yb_xNiSn$ (x=0, 0.01, 0.02, 0.04, 0.06, and 0.10) half-Heusler alloys using a time-efficient levitation melting and spark plasma sintering procedure. They have seen that the electrical conductivity values increased with increasing temperature, showing semiconductor behaviour. The thermal conductivity values decreased and figure of merit values increased depending on the doping and temperature on their samples [30].

4. Conclusion

We have grown semiconducting β-Zn$_4$Sb$_3$ and ZrNiSn-based half-Heusler compound thin films on the silicon and silica substrates using IBAD. Rutherford backscattering spectrometry (RBS) was used to analyze the composition of the thin films. The thin films were then bombarded by 5 MeV Si ions for generation of nanostructures in the films. As we explained in the text, the 5 MeV Si ions bombardment caused increment in the electrical conductivity, decrement in the thermal conductivity, and thus increment in the figure of merit when the suitable fluences of bombardment were chosen. We got the figure of merit of 0.53 for Zn$_4$Sb$_3$ thin film at the fluence of $1*10^{14}$ ions/cm^2. We have reached the figure of merit of 0.20 for Zn$_4$Sb$_3$ thin film at the thickness of 383 nm in our previous study [17]. In the present study we increased the thickness as about two times with respect to the previous study [17], and the figure of merit in the present study increased more than two times. We have reached the figure of merit of 0.0038 for Zn$_4$Sb$_3$ thin film at the fluence of $8*10^{15}$ ions/cm^2. We will continue to get a higher figure of merit for these thin film systems in our future studies using doping of different materials and variation of temperatures.

References

[1] Budak, S., Muntele, C., Zheng, B., Ila, D., 2007, Nuc. Instr. and Meth. B 201, 1167.

[2] Singh, Rajeev, Bian, Zhixi, Shakouri, Ali, Zeng, Gehong, Bahk, Je-Hyeong, Bowers, John E., Zide, Joshua M. O., and Gossard, Arthur C., 2009, Direct measurement of thin-film thermoelectric figure of merit, APPLIED PHYSICS LETTERS 94, 212508.

[3] Hoh, Heinrich, Ramirez, Art P., Goldman, Claudia, Ernst, Gabriele, Wolfing, Bernd, and Bucher, Ernst, 1999, Efficient dopants for ZrNiSn-based thermoelectric materials, J. Phys.: Condens. Matter 11, 1697-1709.

[4] Huang, X. Y., Xu, Z., Chen, L. D., 2004, Solid State Communications 130, 181.

[5] Ito, Kazuhiro, Zhang, Lanting, Adachi, Katsuyuki, and Yamaguchi, Masaharu, 2004, Mater. Res. Soc. Symp. Proc. Vol.793, Materials Research Society S5.1.

[6] Okamura, Chinatsu, Ueda, Takashi, and Hasezaki, Kazuhiro, 2010, Preparation of Single-Phase ZnSb Thermoelectric Materials Using a Mechanical Grinding Process, Materials Transactions, Vol. 51, No. 5, 860-862.

[7] Xiong, Ding-Bang, Okamoto, Norihiko L., and Inui, Haruyuki, 2013, Enhanced thermoelectric figure of merit in p-type Ag doped ZnSb nanostructured with Ag_3Sb, Scripta Materials 69, 397-400.

[8] Zhang, L. T., Tsutsui, M., Ito, K., Yamaguchi, M., 2003, Effects of ZnSb and Zn inclusions on the thermoelectric properties of β-Zn_4Sb_3, Journal of Alloys and Compounds 358, 252-256.

[9] Scales, Brian C., 2002, Science 295, 1248.

[10] Zheng, B., Budak, S., Zimmerman, R. L., Muntele, C., Chhay, B., Ila, D., 2007, Surface & Coatings Technology 201, 8531.

[11] Yoo, B. Y., Huang, C. -K., Lim, J. R., Herman, J., Ryan, M. A., Fleural, J. -P., Myung, N. V., 2005, Electrochemical Acta 50,4371.

[12] Budak, S., Parker, R., Smith, C., Muntele, C., Heidary, K., Johnson, R. B., ILA, D., 2013, Superlattice Multi-nanolayered Thin Films of SiO_2/SiO_2+Ge for Thermoelectric Device Applications, *Journal of Intelligent Material Systems and Structures* 24(11)*, 1357-1364.

[13] Budak, S., Smith, C., Muntele, C., Chhay, B., Heidary, K., Johnson, R. B., ILA, D., 2013, Thermoelectric Properties of SiO_2/SiO_2+CoSb Multi-nanolayered Thin Films Modified by MeV Si Ions, *Journal of Intelligent Material Systems and Structures* 24(11)*, 1350-1356.

[14] Tritt, Terry M., and Subramanian, M.A., 2006, MRS Bulletin 31, 190.

[15] Katsuyama, Shigeru, Matsuo, Ryosuke, Ito, Mikio, 2007, J. Alloys Compd. 428, 262.

[16] Budak, S., Smith, C. C., Zheng, B., Muntele, C. I., Zimmerman, R. L., and Ila, D., 2007, Mater. Res. Soc. Symp. Proc. Vol. 974, Materials Research Society 0974-CC10-16.

[17] Guner, S., Budak, S., Muntele, C., Ila, D., 2009, Surface & Coating Technology 203, 2664-2666.

[18] Holland, L. R., Simith, R. C., 1966, J. Apl. Phys. 37, 4528.

[19] Cahill, D. G., Katiyar, M., Abelson, J. R., 1994, Phys. Rev.B 50, 6077.

[20] Tasciuc, T. B., Kumar, A.R., Chen, G., 2001, Rev. Sci. Instrum. 72, 2139.

[21] Ziegler, J. F., Biersack, J. P., Littmark, U., 1985, The Stopping Range of Ions in solids, Pergamon Press, Newyork, 1985.

[22] Chu, W. K., Mayer, J. W., Nicolet, M. –A., 1978, Backscattering Spectrometry, Academic Press, New York.

[23] Doolittle, L. R., Thompson, M. O., 2002, RUMP, Computer Graphics Service.

[24] Budak, S., Guner, S., Smith, C. C., Muntele, C. I., Zimmerman, R. L., and Ila, D., 2007, Mater. Res. Soc. Symp. Proc. Vol. 1020, Materials Research Society 1020-GG07-09.

[25] Chen, G., Narayanaswamy, A., Dames, C., 2004, Superlattices and Microstructures 35, 161.

[26] Budak, S., Zheng, B., Muntele, C., Xiao, Z., Muntele, I., Chhay, B., Zimmerman, R. L., Holland, L. R., and Ila, D., 2006, Mater. Res. Soc. Symp. Proc. Vol. 929, Materials Research Society 0929-II04-10.

[27] Song, X., Botther, P. H. M., Karlsen, O. B., Finstad, T. G., and Tafto, J., 2012, Impurity band conduction in the thermoelectric material ZnSb, Phys. Scr. T148, 014001 9(6pp).

[28] Muta, Hiroaki, Kanemitsu, Takanori, Kuroski, Ken, and Yamanaka, Shinsuke, 2006, Substitution Effect on Thermoelectric Properties of ZrNiSn Based Half-Heusler Compounds, Materials Transactions, Vol. 47, No.6, 1453-1457.

[29] Qiu, Pengfei, Yang, Jiong, Huang, Xiangyang, Chen, Xihong, and Chen, Lidong, 2010, Effect of antisite defects on band structure and thermoelectric performance of ZrNiSn half-Heusler alloys, Applied Physics Letters 96,152105.

[30] Liu, Xiao-Hua, He, Jian, Xie, Han-Hui, Zhao, Xin-Bing, and Zhu, Tie-Jun, 2012, Fabrication and thermoelectric properties of Yb-doped ZrNiSn half-Heusler alloys, International Journal of Smart and Nano Materials, Vol. 3, No. 1, 64-71.